Structural basis for lipid transport by the MLA complex

Daniel Mann[1,&], Junping Fan[3,%], Daniel P. Farrell[4], Kamolrat Somboon[5], Andrew Muenks[4], Svetomir B. Tzokov[1], Syma Khalid[5], Frank Dimaio[4], Samuel I. Miller[3,4,6,7], Julien R. C. Bergeron[1,2]*

[1] Department of Molecular Biology and Biotechnology, The University of Sheffield, Sheffield, United Kingdom

[2] Randall Division of Cell and Molecular Biophysics, King's College London, London, UK

[3] Department of Microbiology, The University of Washington, Seattle, USA

[4] Department of Biochemistry, The University of Washington, Seattle, USA

[5] Department of Chemistry, University of Southampton, Southampton, UK

[6] Department of Genetics, The University of Washington, Seattle, USA

[7] Department of Medicine, The University of Washington, Seattle, USA

[&] Current address: Ernst-Ruska-Centre 3, Forschungszentrum Jülich, Germany

[%] Current address: Department of Pharmacology, The University of Washington, Seattle, USA

*Correspondence to: julien.bergeron@kcl.ac.uk

Abstract:

The maintenance of lipid asymmetry (MLA) system is involved in lipid transport from/to the outer membrane in gram-negative bacteria, and contributes to broad-range antibiotic resistance. Here, we report the cryo-EM structure of the *A. baumannii* MlaBDEF core complex, in the *apo*, ADP- and AppNHp-bound states. This reveals multiple lipid binding sites, and suggests a mechanism for their transport.

Gram-negative bacteria are enveloped by two lipid bilayers, separated by the periplasmic space containing the peptidoglycan cell wall. The two membranes have distinct lipid composition: The inner membrane (IM) consists of glycerophospholipids, with both leaflets having similar compositions, while the outer membrane (OM) is asymmetric, with an outer leaflet of lipopolysaccharides (LPS) and an inner leaflet of glycerophospholipids (1). This lipid gradient is maintained by several machineries, including YebT, PqiB, and the multicomponent MLA system (2, 3), which consists of MlaA present in the OM (4, 5), the shuttle MlaC in the periplasmic space, and the MlaBDEF ABC transporter system in the IM (6). The directionality of lipid transport by the MLA system has been the subject of debate, with initial reports suggesting that it recycles lipids from the OM to the IM (7), but recent results (6, 8) indicated that it might exports glycerophospholipids to the outer membrane. Low-resolution cryo-EM maps of the MlaBDEF core complex, from *Escherichia coli* (2) and *Acinetobacter baumannii* (6) have revealed the overall architecture of the complex, but did not allow to elucidate the molecular details of lipid binding and transport.

To address the mechanism of MLA functioning, we have determined the cryo-EM structure of the *A. baumannii* MlaBDEF complex, bound to the non-hydrolizable ATP analogue AppNHp, to 3.9 Å resolution (Fig. 1A, Suppl. Fig. 1, Table S1). This allowed us to build an atomic model of the entire complex (Fig. 1B, Table S1, see Supplementary Information for details). We have also obtained cryo-EM maps of this complex in the nucleotide-free state to 4.2 Å, and of the ADP-bound state to 4.4 Å (Fig. 1D, Suppl. Fig. 3, Table S1).

As suggested by the previous low-resolution studies, the transmembrane multiprotein complex features a 6-fold symmetric assembly of MlaD, with the C-terminal helix forming a basket in the periplasmic space, and the N-terminal helix spanning the inner membrane (Fig. 1 A,B, Suppl. Fig. 2 A,B). Similar to other MCE domain proteins (9), MlaD consists of a central beta sheet motif with a central pore loop that is formed by hydrophobic Leu153/Leu154 in the center of the C6 symmetric complex. Cryo-EM maps of MlaBDEF in all three nucleotide states (apo- and bound to AppNHP and ADP) show clear density for six lipid moieties between the central pore loops, as well as a central lipid density (Fig. 1 C,E), that was resolved even when no symmetry was applied during the reconstruction. Similar lipid binding sites were previously observed in the MCE protein YebT (10). The basket region has been proposed to form the binding site for periplasmic MlaC (4), suggesting that lipids are extracted from this position upon MlaC binding. 3D variability analysis (11) indicates that the 6x MlaD crown can be translated and rotated against the MlaBEF transmembrane part (Suppl. Fig. 1), probably limiting achievable resolution for this region of the map. The role of this motion in lipid transport is not currently established. To investigate basic lipid dynamics in the basket region, we performed molecular dynamics simulations, and observed lipid movement towards the central channel within just 50 ns of the 250 ns trajectory (Suppl. Fig. 9), and within 150 ns one lipid

molecule was located within the channel for the remainder of the simulation, suggesting a possible path for lipid translocation upon opening of the complex.

The N-terminal helices of MlaD are wrapped around the two MlaE molecules in the membrane, with three MlaD helices interacting asymmetrically with one MlaE, as reported previously (6). Intriguingly, while MlaE was predicted to have 6 TM helices, we observe that TM1 does not traverse the membrane, but is monotropically embedded in the inner leaflet, a feature similar to the G5G8 human sterol exporter (12), suggesting similar mechanisms between these complexes, and further supporting the MLA system as a lipid exporter.

On the cytosolic side, MlaE is anchored into the ATPase MlaF via the coupling helix situated between TM3 and TM4 (Fig. 1 B, Suppl. Fig. 4 A), again similar to the G5G8 sterol exporter complex. MlaF is bound to MlaB away from the nucleotide binding site, as observed in the recently solved *E.coli* MlaBF crystal structure (13), with C-termini of MlaF binding the opposing MlaB subunit by a “handshake” mode. We note however that particle classification demonstrated that only ~50% of the particles included MlaB bound to both MlaF, leaving the other 50% bound to only one copy of MlaB (Suppl. Fig. 6). Dual binding of MlaB did not introduce major structural alterations at the detected resolution, and this observation may correspond to a regulatory role for MlaB, or could be due to complex disassembly during sample preparation.

The position of the nucleotide binding sites can be clearly identified in the AppNHp-bound map (Fig. 1 D). The nucleotide links the ATPase subunits with the lipid transport domains at the interface of MlaF, MlaE and the N-terminus of MlaD (Suppl. Fig. 5). The resolution was sufficient to map the phosphate binding regions like Walker-A motif around Lys55 of MlaF, as well as binding of γ-GTP by Ser51 and His211 (H-loop). The Mg^{2+}-ion is coordinated by the Walker-B motif around Asp177 (Suppl. Fig. 5) and adenosine ring binding is achieved through Arg26 in the A-loop. As revealed in the previously-reported low-resolution map (6), the position of MlaF suggest that the complex is in the substrate-bound conformation. However, surprisingly, we note no significant conformational changes in the apo and ADP-bound states, other than the nucleotide binding site (Fig. 1 D). This demonstrates that ATP binding or hydrolysis is not sufficient to induce the complex to adopt an outward-facing conformation.

Well-defined densities were also identified between MlaE TM1, and two MlaD helices, within the inner leaflet of the lipid bilayer (Fig. 1 C, yellow), coated by cationic residues, mainly Arg14, Arg47 and Arg234 of MlaE, forming a charged pocket that might attract a lipid head group (Fig. 1 F), leading us to propose that this is the substrate binding pocket. As the sample was solubilized in β-DDM this density is most likely occupied by the maltoside rings of β-DDM, with the flexible hydrophobic chains extending up into an apolar region of MlaE. In this orientation lipids can be directly incorporated from the inner leaflet of the inner membrane and transported

to the MlaD basket, without flipping. This is consistent with the crystal structure of MlaC bound to lipids (8), where the head group is located towards the outside of the protein, indicating that the lipid was loaded hydrophobic-side-first. Molecular dynamics simulations without lipids initially in the binding sites showed rapid incorporation of bulk lipids during equilibration, and stable binding during 500 ns production runs (Suppl. Fig. 8). The C-terminal helices of MlaE directly connect the ATP binding regions of MlaF with the lipid allocrit. As indicated above, all three nucleotide states show comparable density for the bound lipids.

Based on these observations, we propose that nucleotide binding/hydrolysis is not sufficient to trigger lipid translocation. This is consistent with previous biochemical studies (14). We hypothesize that binding of the periplasmic compound MlaC is necessary to trigger allocrit transport (Fig. 2). Lipids can freely access the cationic paired binding sites on the inner leaflet of the inner membrane and are locked mainly by kinked MlaE TM2 and the monotropic MlaE TM1 that block access to the central channel (Fig. 2) and one copy of MlaD that is locked between the MlaE helices (Fig. 2, red). MlaC binding in the basket region could allow direct transfer of one or more of the seven stored lipids. Furthermore, as MlaD directly connects the basket region with nucleotide binding sites and the paired cytosolic lipid binding sites structural alterations would allow opening of the central channel.

Acknowledgments:

We are thankful for financial support through BBSRC project BB/R019061/1. We acknowledge Diamond Light Source for access and support of the cryo-EM facilities at the UK's national Electron Bio-imaging Centre (eBIC) [under proposal EM-19832]. We thank Emma Hasketh and Rebecca Thompson from the Astbury Centre for Structural Molecular Biology Leeds for support during measurements. We acknowledge Nora Cronin for support for data collection at the LonCEM consortium. The University of Sheffield FoS cryo-EM facility was used for grid preparation and optimization. We are grateful to Justin Kollman for help with the initial stages of this project.

Authors contribution:

DM purified the MlaBDEF complex, performed the cryo-EM experiments, and processed the data, with advice from JRCB. DM, DPF and AM built the atomic model, with support from JRCB and FM. KS and SK performed the MD simulation experiments. JF and SIM provided biological insights. DM and JRCB wrote the manuscript, with comments from all the authors.

138 **Reference:**

139 1. Zhang, Y.-M., and Rock, C. O. (2008) Membrane lipid homeostasis in bacteria. *Nat. Rev.*
140 *Microbiol.* **6**, 222–233
141 2. Ekiert, D. C., Bhabha, G., Isom, G. L., Greenan, G., Ovchinnikov, S., Henderson, I. R.,
142 Cox, J. S., and Vale, R. D. (2017) Architectures of Lipid Transport Systems for the
143 Bacterial Outer Membrane. *Cell*. **169**, 273-285.e17
144 3. Isom, G. L., Coudray, N., MacRae, M. R., McManus, C. T., Ekiert, D. C., and Bhabha, G.
145 (2020) LetB Structure Reveals a Tunnel for Lipid Transport across the Bacterial
146 Envelope. *Cell*. **181**, 653-664.e19
147 4. Abellón-Ruiz, J., Kaptan, S. S., Baslé, A., Claudi, B., Bumann, D., Kleinekathöfer, U., and
148 van den Berg, B. (2017) Structural basis for maintenance of bacterial outer membrane
149 lipid asymmetry. *Nat. Microbiol.* **2**, 1616–1623
150 5. Yeow, J., Tan, K. W., Holdbrook, D. A., Chong, Z.-S., Marzinek, J. K., Bond, P. J., and
151 Chng, S.-S. (2018) The architecture of the OmpC–MlaA complex sheds light on the
152 maintenance of outer membrane lipid asymmetry in Escherichia coli. *J. Biol. Chem.* **293**,
153 11325–11340
154 6. Kamischke, C., Fan, J., Bergeron, J., Kulasekara, H. D., Dalebroux, Z. D., Burrell, A.,
155 Kollman, J. M., and Miller, S. I. (2019) The Acinetobacter baumannii Mla system and
156 glycerophospholipid transport to the outer membrane. *eLife*. **8**, e40171
157 7. Malinverni, J. C., and Silhavy, T. J. (2009) An ABC transport system that maintains lipid
158 asymmetry in the gram-negative outer membrane. *Proc. Natl. Acad. Sci. U. S. A.* **106**,
159 8009–8014
160 8. Hughes, G. W., Hall, S. C. L., Laxton, C. S., Sridhar, P., Mahadi, A. H., Hatton, C.,
161 Piggot, T. J., Wotherspoon, P. J., Leney, A. C., Ward, D. G., Jamshad, M., Spana, V.,
162 Cadby, I. T., Harding, C., Isom, G. L., Bryant, J. A., Parr, R. J., Yakub, Y., Jeeves, M.,
163 Huber, D., Henderson, I. R., Clifton, L. A., Lovering, A. L., and Knowles, T. J. (2019)
164 Evidence for phospholipid export from the bacterial inner membrane by the Mla ABC
165 transport system. *Nat. Microbiol.* **4**, 1692–1705
166 9. Isom, G. L., Davies, N. J., Chong, Z.-S., Bryant, J. A., Jamshad, M., Sharif, M.,
167 Cunningham, A. F., Knowles, T. J., Chng, S.-S., Cole, J. A., and Henderson, I. R. (2017)
168 MCE domain proteins: conserved inner membrane lipid-binding proteins required for
169 outer membrane homeostasis. *Sci. Rep.* **7**, 1–12
170 10. Liu, C., Ma, J., Wang, J., Wang, H., and Zhang, L. (2020) Cryo-EM Structure of a
171 Bacterial Lipid Transporter YebT. *J. Mol. Biol.* **432**, 1008–1019
172 11. Punjani, A., and Fleet, D. J. (2020) 3D Variability Analysis: Directly resolving continuous
173 flexibility and discrete heterogeneity from single particle cryo-EM images. *bioRxiv*.
174 10.1101/2020.04.08.032466

12. Lee, J.-Y., Kinch, L. N., Borek, D. M., Wang, J., Wang, J., Urbatsch, I. L., Xie, X.-S., Grishin, N. V., Cohen, J. C., Otwinowski, Z., Hobbs, H. H., and Rosenbaum, D. M. (2016) Crystal structure of the human sterol transporter ABCG5/ABCG8. *Nature*. **533**, 561–564
13. Structure of MlaFB uncovers novel mechanisms of ABC transporter regulation | bioRxiv [online] https://www.biorxiv.org/content/10.1101/2020.04.27.064196v1.full (Accessed May 2, 2020)
14. Thong, S., Ercan, B., Torta, F., Fong, Z. Y., Wong, H. Y. A., Wenk, M. R., and Chng, S.-S. (2016) Defining key roles for auxiliary proteins in an ABC transporter that maintains bacterial outer membrane lipid asymmetry. *eLife*. **5**, e19042

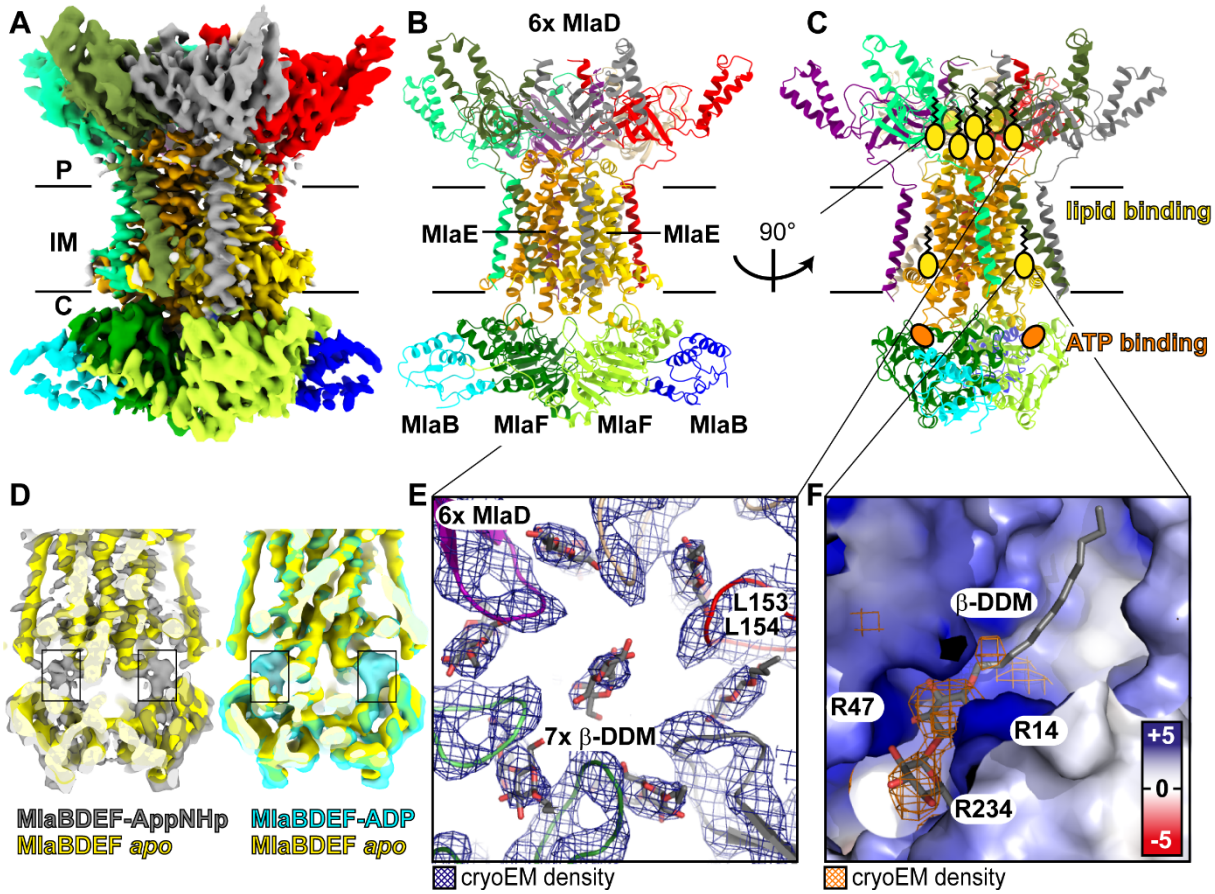

Figure 1: A: 3.9 Å Cryo-EM map of MlaBDEF-AppNHp in β-DDM (C=cytosol, IM=inner membrane, P=periplasm). B: MlaBDEF has global C2 symmetry with six copies of MlaD that span the inner membrane from the periplasmic space to the cytosol, two copies of MlaE embedded in the membrane (yellow/gold), two copies of the ATPase MlaF in the cytosol (green), each bound to a copy of MlaB (blue/cyan). C: when rotated 90° within the membrane plane MlaBDEF houses paired binding sites for lipids (yellow) and nucleotides (orange). The periplasmic part forms a basket that binds 6 peripheral and one central lipid. D: Nucleotide binding sites were verified by solving the structures of MlaBDEF-AppNHp (grey), MlaBDEF-ADP (cyan) and MlaBDEF-apo (yellow) The apo map lacks nucleotide density that is indicated by boxes. E: Close-up of the periplasmic MlaD basket that houses six peripheral and one central lipid. F: Electrostatic surface potential of modeled inner membrane MlaBDEF (blue=+5 kT/e, white=0kT/e, red=-5kT/e) shows a cationic binding site for anionic lipid head groups like β-DDM and an apolar pocket for the uncharged lipid tails. β-DDM was modeled inside the map density (orange mesh).

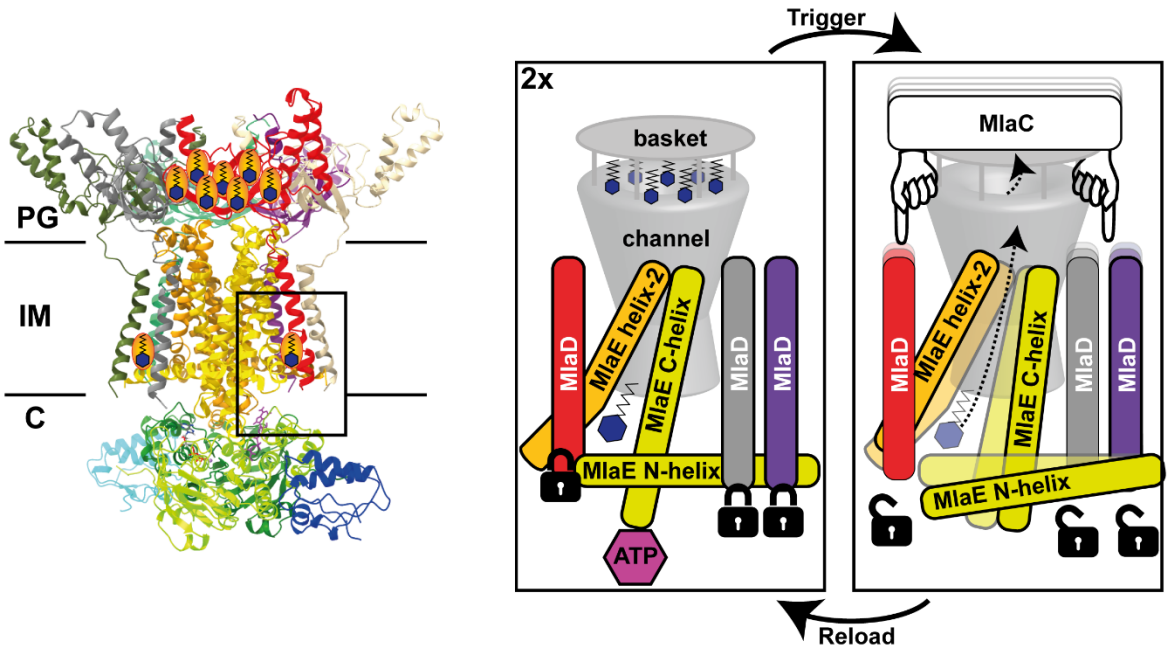

201

202 **Figure 2:** Proposed mechanism for lipid transport by MlaBDEF. The lipid (blue) is locked by
203 MlaD (red), MlaE helix-2 (gold), the MlaE C-helix (yellow) and the perpendicular MlaE N-helix
204 (yellow) in the apo- as well as the ADP- and the AppNHp-bound state. As MlaD proteins (red,
205 grey, purple) connect the cytosol with the periplasmic space, docking of MlaC (white) can
206 directly open this locked conformation and release the allocrit through the central channel
207 that is formed by the MlaD hexamer.

208

209 **Online methods:**

210 MlaBDEF protein expression and purification

211 *Acinetobacter baumannii* ATCC 17978 MlaBDEF was cloned into the pET-28a vector with a
212 C-terminal Hexahistidine tag at MlaB, as described previously (6). The plasmid was
213 transformed into *Escherichia coli* BL21 DE3 cells and grown at 37°C until the cell density
214 reached OD(600nm) = 1.0. The temperature was reduced to 20°C before induction with 1 mM
215 isopropyl β-D-thiogalactoside (IPTG) and incubation overnight. Cells were harvested using
216 centrifugation at 5000 x g and resuspended in ice-cold buffer A (20 mM Tris-HCl (pH 8.0), 150
217 mM NaCl, 5% (v/v) glycerol) before disruption in an ultrasonicator on ice (6 cycles; 60s run,
218 30s cooldown). Cell debris was centrifuged down at 17,000 x g for 10 min and the supernatant
219 was centrifuged at 100,000 x g for 1h. This pellet was resuspended by gentle stirring in Buffer
220 A supplemented with 1% (w/v) dodecyl-β-d-maltopyranoside (β-DDM) at 7°C for 1 h. After
221 another centrifugation step at 100,000 x g for 30 min the supernatant was applied to a 5 ml Ni-
222 NTA superflow column (GE Healthsciences) that was previously equilibrated with ddH_2O and
223 buffer A supplemented with 20 mM imidazole and 0.025% (w/v) β-DDM. The column was
224 washed with buffer A supplemented with 20 mM imidazole and 0.025% (w/v) β-DDM before
225 elution with buffer A supplemented with 300 mM imidazole and 0.025 % (w/v) β-DDM was
226 performed. The elute was concentrated to 5 ml and applied to a gel filtration run on a 16-600
227 HiLoad Superdex 200 pg column (GE Healthcare), preequilibrated with 20 mM Hepes (pH 7.0),
228 150 mM NaCl, 0.025% (w/v) β-DDM. Peak fractions were collected, purest fractions were
229 selected using SDS-PAGE and concentrated to 5 mg/ml.

230 CryoEM sample preparation, data acquisition and image processing

231 4 µl freshly purified 5 mg/ml MlaBDEF in 20 mM Hepes (pH 7.0), 150 mM NaCl, 0.025% (w/v)
232 β-DDM was applied on 30s freshly glow discharged 300 mesh Quantifoil R2/2 grids, blotted for
233 3.5 s in a Leica EM-GP plunge freezer at 80% humidity and 4°C, before getting plunged into
234 liquid ethane at -170 °C. For investigation of the AppNHp and ADP states, the protein was
235 mixed 1:1 with 20 mM of the corresponding nucleotide in 50 mM Hepes (pH 8.0), 150 mM
236 NaCl, 0.025 % (w/v) b-DDM buffer and incubated for 60 min on ice prior to grid preparation.

237 Micrographs of MlaBDEF-AppNHp were recorded on a 300 kV Titan Krios microscope with a
238 Gatan K2 Summit detector in counting mode. 2557 movies were recorded with a pixel size of
239 1.07 Å in 47 frames with $1e^-/Å^2$/frame. 1901 movies of MlaBDEF-ADP were recorded on the
240 same instrument with a total dose of 40 $e^-/Å^2$. The MlaBDEF apo dataset was recorded on a
241 300 KV Titan Krios equipped with a Gatan K3 bioquantum detector. 4737 micrographs with a
242 pixel size of 0.41 Å were recorded with a total dose of 40 $e^-/Å^2$ in 50 frames. Data processing
243 was performed in CryoSPARC v2.14.2 (see Supplemental Figures 1 and 3 for details). Raw

244 images of the MlaBDEF-AppNHp dataset are publicly available under EMPIAR-10425.
245 Sharpened maps in C2, C1 and C6 symmetry, masks and half-maps of MlaBDEF-AppNHp, -
246 ADP and apo are publicly available under EMD-11082, EMD-11084 and EMD-11083,
247 respectively.

248 Model building

249 The structural model of MlaBDEF was manually built into the high-resolved regions of the
250 MlaBDEF-AppNHp map using Coot. Computational intervention was required to build residues
251 4-38, and 94-134 of MlaD, as well as refine the AppNHp binding site of MlaF. RosettaES (1)
252 was used to model residues 4-38 for each of the 6 MlaD subunits using the manually built
253 model as the starting point. Residues 94-134 were first modeled with Rosetta *Ab-initio* (2)
254 which yielded a tightly converged ensemble with a 2-helix topology. The top scoring model
255 from the *Ab-initio* predictions was unambiguously docked into the corresponding density for
256 each of the MlaD subunits using UCSF Chimera (3). Loops were completed and the entire
257 MlaD crown refined using RosettaCM (4) with the context of the cryoEM density. To refine the
258 AppNHp binding site of MlaF we first used RosettaCM to hybridize the manually built model
259 with the homologous structures of (3fvq, chain A), and (4ki0, chain B) in the cryoEM density.
260 Then using homology models and the unexplained density as a guide, a modified version of
261 the rosetta protocol GALigandDock (unpublished) that uses the cryoEM data to drive sampling
262 was used to dock the AppNHp molecule. As input to the protocol, a mol2 file of AppNHp was
263 modified using openbabel (v. 2.4.1) (5) to add hydrogens, charges were assigned with the
264 AM1-BCC charge method in antechamber (6) and a params file was generated with the script
265 `main/source/scripts/python/public/generic_potential/mol2genparams.py`
266 which is distributed with Rosetta. Finally, the entire complex was refined using RosettaCM,
267 and Magnesium atoms were added by incorporating distance and angle constraints between
268 the Mg atoms and the AppNHp oxygens on the β and γ phosphates during the final
269 minimization. ISOLDE in ChimeraX was used to manually correct for modeling errors.
270 Phenix.real.space.refine was used for refinement and validation. The MlaBDEF-AppNHp
271 model is publicly available under PDB-6Z5U.

272 Molecular dynamics system preparation

273 The Mla Cryo-EM structure was completed by adding the missing residues using Modeller 9.23
274 (http://salilab.org/modeller/)(7, 8). A system, having the completed protein structure embedded
275 in an inner *E.coli* innermembrane, was generated with the CHARMM GUI web interface(9–15)
276 to have dimensions of ~21 × 21 × 18 nm. The inner membrane composition was based on
277 previous atomistic simulations studies(16): 75% 1-palmitoyl-2-oleoyl-sn-glycero-3-
278 phosphoethanolamine (POPE), 20% 1-palmitoyl-2-oleoyl-sn-glycero-3-phosphoglycerol
279 (POPG) and 5% 1′,3′-bis[1,2-dioleoyl-sn-glycerol-3-phospho-]-sn-glycerol (Cardiolipin). To

280 relax any steric conflicts within the system generated during set up, energy minimization of
281 5000 steps was performed on the starting conformation using the steepest descent method.
282 An equilibration procedure followed in which the protein was subjected to position restraints
283 with different force constant. The full equilibration protocol is shown in table S2. Two different
284 scenarios were simulated, one in which the protein was simply embedded into the membrane
285 as described above (Mla), and one in which seven additional POPE lipids were placed around
286 the entrance of Mla corresponding to the density for detergents in the cryo-EM data ($Mla_{_7PE}$),
287 the additional lipids were placed using Visual Molecular Dynamics (VMD)(17)

288 Equilibrium molecular dynamics simulations

289 All simulations were carried out with GROMACS 2019.6(18) version (www.gromacs.org) and
290 CHARMM36(19) forcefield. For the nonbonded interactions and the short-range electrostatics
291 cut offs of 1.2 nm was applied to the system with the potential shift Verlet cut off scheme,
292 whereas the long-range electrostatic interactions were treated using the Particle Mesh Ewald
293 (PME) method(20). All atoms were constrained using the LINCS algorithm(21) to allow the
294 time step of 2 fs. The desired temperature at either 310 K or 323 K was controlled with Nose-
295 hoover thermostat(22, 23) using a coupling constant of 1.0 ps coupling constant. The pressure
296 was maintained at 1 atm using the Parrinello-Rahman(24) semi-isotropic barostat with a
297 coupling constant of 1.0 ps. Equilibrium MD systems were performed with two repeats. Each
298 repeat was run with different initial velocities. The summary of all production runs is shown in
299 table S3. The results were analysed using built-in functions within GROMACS. Molecular
300 images were prepared with VMD.

301

302

303 **Online methods references:**

304 1. B. Frenz, A. C. Walls, E. H. Egelman, D. Veesler, F. DiMaio, RosettaES: a sampling
305 strategy enabling automated interpretation of difficult cryo-EM maps. *Nat. Methods* **14**,
306 797–800 (2017).
307 2. K. T. Simons, R. Bonneau, I. Ruczinski, D. Baker, Ab initio protein structure prediction of
308 CASP III targets using ROSETTA. *Proteins Struct. Funct. Bioinforma.* **37**, 171–176
309 (1999).
310 3. E. F. Pettersen, *et al.*, UCSF Chimera—A visualization system for exploratory research
311 and analysis. *J. Comput. Chem.* **25**, 1605–1612 (2004).
312 4. Y. Song, *et al.*, High-Resolution Comparative Modeling with RosettaCM. *Structure* **21**,
313 1735–1742 (2013).
314 5. N. M. O'Boyle, *et al.*, Open Babel: An open chemical toolbox. *J. Cheminformatics* **3**

(2011).
6. J. Wang, W. Wang, P. A. Kollman, D. A. Case, Automatic atom type and bond type perception in molecular mechanical calculations. *J. Mol. Graph. Model.* **25**, 247–260 (2006).
7. Šali, A., and Blundell, T. L. (1993) Comparative Protein Modelling by Satisfaction of Spatial Restraints. *J. Mol. Biol.* **234**, 779–815
8. Sánchez, R., and Šali, A. (2000) Comparative Protein Structure Modeling: Introduction and Practical Examples with Modeller. in *Protein Structure Prediction*, pp. 97–129, Humana Press, New Jersey, 10.1385/1-59259-368-2:97
9. Jo, S., Kim, T., Iyer, V. G., and Im, W. (2008) CHARMM-GUI: A web-based graphical user interface for CHARMM. *J. Comput. Chem.* **29**, 1859–1865
10. Brooks, B. R., Brooks, C. L., Mackerell, A. D., Nilsson, L., Petrella, R. J., Roux, B., Won, Y., Archontis, G., Bartels, C., Boresch, S., Caflisch, A., Caves, L., Cui, Q., Dinner, A. R., Feig, M., Fischer, S., Gao, J., Hodoscek, M., Im, W., Kuczera, K., Lazaridis, T., Ma, J., Ovchinnikov, V., Paci, E., Pastor, R. W., Post, C. B., Pu, J. Z., Schaefer, M., Tidor, B., Venable, R. M., Woodcock, H. L., Wu, X., Yang, W., York, D. M., and Karplus, M. (2009) CHARMM: The biomolecular simulation program. *J. Comput. Chem.* **30**, 1545–1614
11. Lee, J., Cheng, X., Swails, J. M., Yeom, M. S., Eastman, P. K., Lemkul, J. A., Wei, S., Buckner, J., Jeong, J. C., Qi, Y., Jo, S., Pande, V. S., Case, D. A., Brooks, C. L., MacKerell, A. D., Klauda, J. B., and Im, W. (2016) CHARMM-GUI Input Generator for NAMD, GROMACS, AMBER, OpenMM, and CHARMM/OpenMM Simulations Using the CHARMM36 Additive Force Field. *J. Chem. Theory Comput.* **12**, 405–413
12. Wu, E. L., Cheng, X., Jo, S., Rui, H., Song, K. C., Dávila-Contreras, E. M., Qi, Y., Lee, J., Monje-Galvan, V., Venable, R. M., Klauda, J. B., and Im, W. (2014) CHARMM-GUI *Membrane Builder* toward realistic biological membrane simulations. *J. Comput. Chem.* **35**, 1997–2004
13. Jo, S., Lim, J. B., Klauda, J. B., and Im, W. (2009) CHARMM-GUI membrane builder for mixed bilayers and its application to yeast membranes. *Biophys. J.* **97**, 50–58
14. Jo, S., Kim, T., and Im, W. (2007) Automated Builder and Database of Protein/Membrane Complexes for Molecular Dynamics Simulations. *PLoS ONE*. **2**, e880
15. Lee, J., Patel, D. S., Ståhle, J., Park, S. J., Kern, N. R., Kim, S., Lee, J., Cheng, X., Valvano, M. A., Holst, O., Knirel, Y. A., Qi, Y., Jo, S., Klauda, J. B., Widmalm, G., and Im, W. (2019) CHARMM-GUI Membrane Builder for Complex Biological Membrane Simulations with Glycolipids and Lipoglycans. *J. Chem. Theory Comput.* **15**, 775–786
16. Holdbrook, D. A., Huber, R. G., Piggot, T. J., Bond, P. J., and Khalid, S. (2016) Dynamics of Crowded Vesicles: Local and Global Responses to Membrane Composition. *PLOS ONE*. **11**, e0156963

17. Humphrey, W., Dalke, A., and Schulten, K. (1996) VMD: visual molecular dynamics. *J. Mol. Graph.* **14**, 33–8, 27–8
18. Van Der Spoel, D., Lindahl, E., Hess, B., Groenhof, G., Mark, A. E., and Berendsen, H. J. C. (2005) GROMACS: Fast, flexible, and free. *J. Comput. Chem.* **26**, 1701–1718
19. Huang, J., and MacKerell, A. D. (2013) CHARMM36 all-atom additive protein force field: Validation based on comparison to NMR data. *J. Comput. Chem.* **34**, 2135–2145
20. Essmann, U., Perera, L., Berkowitz, M. L., Darden, T., Lee, H., and Pedersen, L. G. (1995) A smooth particle mesh Ewald method. *J. Chem. Phys.* **103**, 8577–8593
21. Hess, B., Bekker, H., Berendsen, H. J. C., and Fraaije, J. G. E. M. (1997) LINCS: A linear constraint solver for molecular simulations. *J. Comput. Chem.* **18**, 1463–1472
22. Hoover, W. G. (1985) *Canonical dynamics: Equilibrium phase-space distributions*
23. Nosé, S. (1984) A molecular dynamics method for simulations in the canonical ensemble. *Mol. Phys.* **52**, 255–268
24. Parrinello, M., and Rahman, A. (1981) Polymorphic transitions in single crystals: A new molecular dynamics method. *J. Appl. Phys.* **52**, 7182–7190